A vapor barrier Couette shear cell for small angle neutron scattering measurements

L. Porcar,[a] W. A. Hamilton,[b] and P. D. Butler[c]
Solid State Division, Oak Ridge National Laboratory, Oak Ridge, Tennessee 37831-6393

G. G. Warr
School of Chemistry, University of Sydney, NSW 2006, Australia

(Received 10 October 2001; accepted for publication 11 March 2002)

We describe the design and operation of a temperature controlled Couette shear cell for small angle neutron scattering (SANS) studies of complex fluids under flow. This design incorporates a vapor barrier, which prevents sample evaporation to relatively high shear rates. This cell enables the investigation of systems which are highly sensitive to evaporation. Over the duration of a Couette SANS measurement composition phase transitions due to evaporation can be misinterpreted as true shear-induced transformations. We give a brief report of recent experiments performed on one such system: bicontinuous L_3 sponge phases for which the surfactant membrane constituents are Cetylpyridinium chloride and hexanol. These clearly demonstrate the limitations of previous designs and the utility of the vapor barrier in measurements of a predicted shear induced sponge to lamellar phase transition. Using this cell we also describe and test a simple and effective way to put SANS data taken in the tangential Couette configuration on an absolute scale. © *2002 American Institute of Physics.* [DOI: 10.1063/1.1475351]

I. INTRODUCTION

Since the first report by Ackerson *et al.*[1] of shear induced melting in a colloidal phase containing long ranged order, much attention has been focused on shear-induced structures and transformations in complex fluids. Use of shear as a quasithermodynamic variable, in a manner analogous to control of true thermodynamic parameters such as pressure or temperature, has allowed the observation of a wide variety of shear-induced transformations in such systems.[2] A partial list also includes: shear-induced isotropic to nematic transformations,[3] shear-induced micellar elongation, alignment of rodlike micelles,[4] and the striking lamellar to multilamellar vesicle transitions.[5,6] We are just beginning to come to terms with the richness of the structural responses to shear exhibited by complex fluids. In the last case, for instance, it has been shown that the size of the multilamellar vesicles is correlated with both the shear rate[7] and the shear stress[8] applied to the lamellar phase. Further, under appropriate conditions, this vesicle phase can lead to long-range order corresponding to the crystallization of the so-called spherulite structure.[9] Beyond any fundamental scientific interest, shear is also of great technological interest since shear-induced complex fluid phases may have profound effects on industrial materials processing.

A wide variety of shearing devices have been developed to study shear-induced behavior *in situ* using x-ray and neutron scattering techniques, most notably for exploring polymer solution behavior. A number of different geometries have been used: elongational flow and extrusion, Couette shear between sliding plates, concentric cylinders, cone and plate systems and parallel disks, and Poiseuille surface shear, most corresponding to commonly encountered processing conditions.[10–18] For bulk structural studies using neutrons or x rays, the most commonly used device is the Couette geometry shear cell in which a liquid sample is continuously sheared between two concentric cylinders, one of which rotates while the other is stationary. The average applied shear rate $\dot{\gamma}$ on the sample is the difference in speeds of the inner surfaces of the cylinders divided by the width of the sample gap. So $\dot{\gamma} \approx 2\pi R f/g$, where R is the radius of the fluid annulus, g is the gap width, and f is the cylinder's rotation frequency. This geometry is particularly well suited to fundamental studies of shear responses of low viscosity systems and high shear rates, and devices of this type began to become available at scattering facilities in the early 1980s. Its utility stems from the fact that it provides a relatively simple and easily understood flow field while presenting a reasonably large sheared sample volume and easy access to the probe radiation.

Over the years Couette cells have proved to be an invaluable tool for the investigation of the effects of shear on complex systems. However, with the increasing interest in phases that exist only in restricted regions of the phase diagram, the need for carefully controlled environments has also increased. While temperature has been addressed since the earliest days, it being recognized that some viscous heating of the sample will necessarily occur, the issue of preventing evaporation has received less attention. Some researchers (including our group) have incorporated simple vapor barrier designs on Couette scattering cells. In our experience these devices, while helpful, work effectively only at low shear

[a]Electronic mail: PorcarL@ornl.gov
[b]Electronic mail: HamiltonWA@ornl.gov
[c]Electronic mail: ButlerPD@ornl.gov

rates and are generally inadequate when a sample is sensitive to evaporation. The principal advantage of the cell presented here over previous designs,[10,11,14] is its second generation, active vapor barrier design which prevents evaporation over a much larger range of shear. We have found that use of this barrier allows shear rates up to 15 000 s^{-1} to be maintained for long periods without significant evaporation. Other important features of the design include temperature control and relatively small sample volumes for a neutron scattering cell (as low as 7 ml).

As an example of the potential of our cell, we briefly report on some recent results obtained from two similar sponge phase systems: Cetylpyridinium chloride (CPCl)/hexanol/brine and CPCl/hexanol/brine/dextrose. The first system has been extensively studied,[19–22] and has recently been the subject of x-ray scattering measurements by Majhoub *et al.*,[23] which were interpreted as the observation of sponge to lamellar transitions induced by flow at unexpectedly low shear rates. Our own experiments performed on this system contradict these results and clearly demonstrate the efficiency and utility of this new vapor barrier design, and lead us to reinterpret these earlier results as a simple composition driven phase change due to evaporation.[24] We also present preliminary results on the second evaporation sensitive system, the dextrose sweetened sponge, which does show clear evidence of a shear induced sponge to lamellar transformation. In contrast to the reported transition in the first system, these results can be generally understood in terms of current theories.

II. CELL DESCRIPTION

Many of the design features of our cell follow from the operational considerations comprehensively outlined by Lindner and Oberthur[10] in their design of a neutron Couette shear cell for the Institute Laue Langevin in 1984. Our device can be divided into two main parts: the support and alignment frame and the Couette cell itself. Figure 1 shows a photograph of the ORNL Couette cell installed at the sample position of the NG3 small angle neutron scattering instrument at National Institute of Standards and Technology (NIST) Center for Neutron Research.

A view of the frame with the cell is shown in Fig. 2. The total height of the apparatus is 70 cm. The mounting and alignment assembly for the stationary inner cylinder of the Coutte cell is mounted on a horizontal (black anodized) aluminum plate attached at right angles to a vertical translation stage. This allows it to be precisely lowered within the rotating outer cylinder and raised up to 20 cm above it for cleaning and sample loading. The rotation bearing for the outer cylinder is mounted in an aluminum block and defines the primary (fixed) rotation axis of the cell. The bearing shaft is directly connected to the motor or a gear reducer connected to the motor. The dc motor is connected to a tachometer, which provides accurate monitoring of the rotation speed and consequently shear rate in the cell. The controller is interfaced to the instrument computer (PC) which provides complete remote control operation and monitoring of the cell during data acquisition.

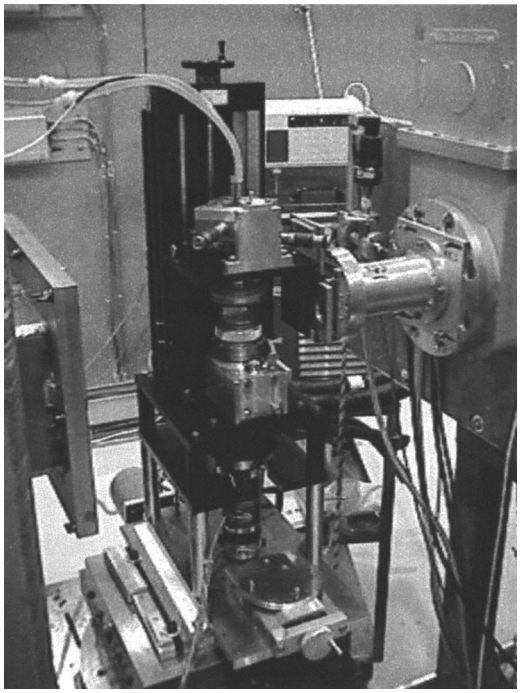

FIG. 1. ORNL Couette shear cell installed at the NG3 SANS instrument sample position at the NIST Center for Neutron Research.

Our Couette cell design comprises an inner stationary cylinder (the stator) and an outer rotating cylinder (the rotor). Both cylinders are fused silica (Suprasil[25]) which has excellent optical qualities and is highly transparent to cold neutrons. The cylinders are 2 mm thick and their optically polished inner and outer surfaces have a radius tolerance along their length of 0.01 mm. Figure 3(a) shows a schematic view

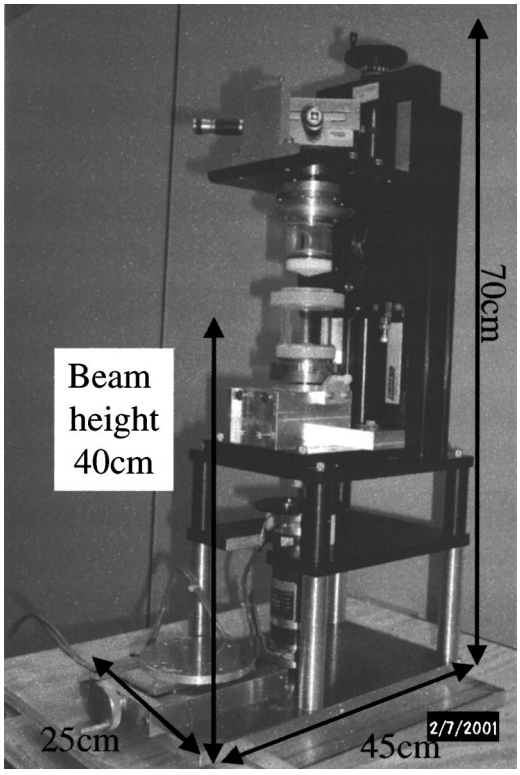

FIG. 2. Couette cell frame with stator raised above rotor.

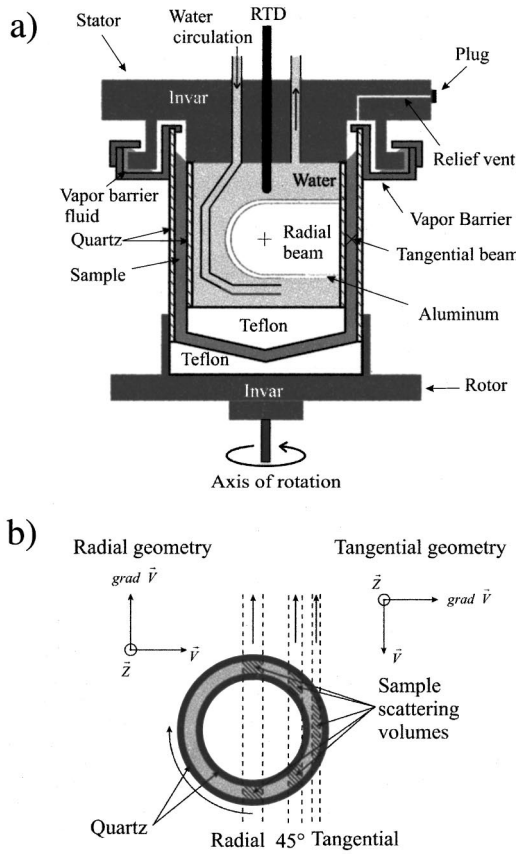

FIG. 3. (a) Schematic view of ORNL Couette sample cell. (b) Top view of the shear cell with the neutron beam passing through the sample annulus in radial, tangential, and intermediate 45° configurations.

of the Couette sample cell. The bottoms of the stator and rotor, which also make contact with the sample, are made of Teflon in order to maximize the chemical resistance while minimizing the complexity of the design. The bottom of the stator is a shallow cone (15°) in order to minimize trapping of air bubbles when it is lowered into position. The rotor bottom has a matching conical cup shape in order to minimize the required sample volume. These Teflon bottoms are slip fits to their respective cylinders and sealed with Teflon encapsulated O rings.[26] To increase the range of shear rates accessible with the cell we have stators with outer radii of 24.50 and 24.00 mm. Within the 25.00 mm inner radius of the rotor this allows Couette sample gaps of 0.50 and 1.00 mm, corresponding to Couette gap ratios, g/R, of 0.02 and 0.04, respectively. These dimensions represent a compromise between keeping the total sample load volume for the cell reasonably small, while minimizing cell curvature (to avoid curvature of the shear field over the scattering volume) and the variation of the shear rate across the gap. For a Newtonian fluid (viscosity is independent of shear rate) the shear rate in a Couette cell actually varies across the gap as $\dot{\gamma}[r] \cong dv/dr \propto r^{-2}$, where r is the distance from the cell axis within the sample annulus.[27] To first order the change in the gradient over the gap is then approximately twice the gap ratio, so for our 0.50 and 1.00 mm gaps about 4% and 8%, respectively—in that simplest case. Such effects, which can be somewhat larger for complex fluid shear responses, are the dominant limit to precision for Couette shear rates in scattering studies. (Motor and hence cylinder rotation speeds are easily determined to a few percent.) Fortunately structural shear responses in the fluids studied generally vary over much larger shear rate ranges. For the 0.50 and 1.00 mm gaps the sample load volumes are 7 and 14 ml, respectively.

While rotating the outer cylinder makes the cell design more difficult, it avoids the problem of Taylor vortex flow being established at relatively low Reynolds number in our cell. For the Couette geometry $\mathrm{Re} \equiv \rho \dot{\gamma} g^2/\eta$, where ρ and η are the density and viscosity of the sample fluid, respectively. For inner cylinder rotation the nonlaminar Taylor flow pattern is fully established at $\mathrm{Re}_T \approx 41.2\sqrt{R/g}$.[28] For our 1.00 mm gap Re_T is then only ~200. (The practical implications of Re limits for general samples may easily be estimated by scaling from water, $\rho = 1\ \mathrm{g\,cm^{-3}}$ and $\eta \approx 1$ cP, for which we note that for a 1 mm gap the shear rate in $\mathrm{s^{-1}}$ will be numerically equal to Re, i.e., so in this case $\dot{\gamma}_T \approx 200\ \mathrm{s^{-1}}$.) For outer cylinder rotation Taylor vortex flow is not established and the operational limit is the critical Reynolds number for the onset of turbulent flow in the annulus,[10,29] typically $\mathrm{Re}_{CR} \sim 1500$. This is an important consideration for neutron Couette cell design, since the large gap necessary to ensure sufficient sample volume results in both a lower Re_T limit and a higher Re for a given sample shear rate. For smaller gap instruments, including most rheological and x-ray cells, the limitation is less serious and in most of these designs an inner cylinder (the bob) rotates while the outer cylinder (the cup) is fixed.

The stator hangs from an aluminum frame supported on a main horizontal plate through two horizontal differential micrometer translation stages at right angles and a precision tilt stage. This mounting allows fine control of the position and angle of the stator cylinder. The rotor cylinder assembly is mounted directly on the rotation bearing, with the quartz cylinder axis precisely collinear with the bearing axis. This is achieved by adjusting the cylinder's axis tilt and position while it is relatively loosely held in its Invar base by an external O ring at its base clamped with a screw cap. Alignment accuracy is determined using dial indicator sensors mounted on the stator mount reaching to the cylinder's inner surface. With care and time the cylinder can be aligned by touch to an accuracy of better than 0.01 mm as the cylinder is rotated, and variation of 0.01–0.02 mm as the dial indicator is moved up by raising the stator mount over the full stator height (~5 cm). This is the accuracy we would expect from the fabrication tolerance of the cylinder and the linearity of the translation stage. To preserve that alignment the rotor cylinder is then glued with epoxy to its Invar mount. The stator is aligned using a dial sensor mounted on the rotation axis reaching to the stator cylinder surface. Using the stator mount's tilt and translation adjustments this alignment is achieved in a similar manner to the rotor alignment and to the same degree of accuracy by rotating the dial indicator around the top and bottom of the outside stator cylinder by raising and lowering the stator. Since the stator is held over the rotor about 10 cm above its operating position to allow space for dial indicator access during this procedure, its accuracy is limited by the precision of the vertical translation stage's alignment with the bearing axis. In the raised

alignment position stator and rotor axes are collinear. While the axes remain highly parallel when the stator is lowered into the rotor, any slight misalignment between the fixed stage translation and the bearing will introduce a slight *position* offset. Final alignment of the stator and rotor axes in the fully lowered measurement position is achieved by a simple fluid dynamic test. The sample annulus is filled to the neutron beam height with a low viscosity liquid (e.g., methanol). When the Couette cell is operated at the rotation speeds of interest any residual misalignment will result in a tilted or unstable meniscus. Provided the initial alignment has been correctly performed only a little fine tuning (repeatable to less than 0.005 mm) of the stator translation stage adjustments (and very rarely the tilt adjustments) is necessary to bring the meniscus to stable and level. This final alignment results in a sample gap which varies by $\sim$0.01 mm over the neutron beam height ($\sim$1 cm) as the outer cylinder rotates. This is simply the sum of the fabrication errors in both inner and outer quartz surfaces of the fluid annulus, corresponding to variations in the gap width of $\sim$2% and $\sim$1% for the 0.50 and 1.00 mm gaps, respectively.

The major advantage of our Couette cell is its vapor barrier design, which greatly improves the sealing of the sample volume against evaporation. Initial vapor barrier designs for neutron Couette cells (including our own) have employed a simple annular vertical vane and well system. In this arrangement the vane is mounted outside the stator and the liquid-filled well is mounted at the top of the rotor. When the stator is lowered the vane dips into the well fluid, sealing off the volume above the sample. Our second-generation vapor barrier is designed and operated to correct the deficiencies we have experienced with this original design, which was effective only at lower shear rates and for samples that were relatively insensitive to evaporation. As the Couette cell spins, centrifugal force pushes the vapor barrier fluid to the outside of the annulus and tilts its surface, lowering the depth at which a vertical vane can penetrate into the barrier fluid. At high rotation speeds it is simply expelled from the well leaving the sample open to the outside environment.

To avoid these mechanical effects we have made the modifications to this design visible in Fig. 3(a). At the bottom of our new sealing vane there is a right angle flange which reaches outward into a wider barrier well. The new well is sealed against centrifugal leakage by a flange cap on top of the well extending toward the stator vane. To allow the stator vane to lift out of the barrier well this cap makes a grease-sealed slip fit to the well. Since the vapor barrier seals before the stator is fully lowered to the measurement position, a relief vent line allows air to be released from above the sample. This prevents trapped air overpressuring the volume enclosed above the sample and forcing out the vapor barrier fluid. With the stator fully lowered this hole is plugged to isolate the volume above the sample during the measurement. The angled vane design does increase the complexity of the design somewhat, requiring the barrier well to be wider than for a simple vertical vane and adding the extra mass of the sealing cap. Our original vapor barrier well was an easily removable O-ring slip fit to the top of the rotor. It was necessary to glue the new heavier well into position to avoid loss of alignment, which limited the rotor's stability at higher rotation speeds.

The mechanical operation of this design is illustrated in the detail of Fig. 3(a), which shows how the seal is maintained for a vapor barrier fluid represented under centripetal acceleration of about 1 G, i.e., the average angle of the barrier liquid meniscus to the horizontal is 45°. For the $\sim$3 cm radius of the well this occurs at a rotation speed of about 200 rpm, corresponding to shear rates of about 500 and 1000 s^{-1} for the 1.00 and 0.50 mm sample gaps, respectively. Even at these relatively low shear rates, it is clear that without the angle on the barrier vane and the well cap it would be difficult to maintain sufficient depth in the vapor seal as increasing centrifugal force begins to force fluid out of the barrier channel. Ideally the vapor barrier should be loaded with a fluid with the same partial vapor pressures as the sheared sample. In practice we have found that loading the vapor barrier with a mixture of the high vapor pressure components of the sample (in the situation presented below a mixture of hexanol in water) is sufficient to eliminate evaporation effects. These mechanical and operational improvements greatly increase the effectiveness of the vapor barrier and high shear rates can be achieved for extended periods. The Couette cell can be driven either in manual or programmed mode. The latter case and the efficiency of the vapor barrier allow us to run the system unsupervised for many hours. In Sec. IV we will briefly describe experiments illustrating the performance of our cell during measurements on samples that are extremely sensitive to evaporation.

Our stator has been specially designed to allow neutron scattering measurements from a Couette sheared sample over a range of configurations from the so-called radial configuration limit, where the incident beam is parallel to the velocity gradient, to the tangential, where the incident beam is parallel to the flow direction, as illustrated in Fig. 3(b). To ensure the best possible thermal regulation of the sample, the thermostating fluid (water or ethylene glycol) circulated within the stator makes direct contact with the quartz cylinder. The open beam path volume necessary for this range of scattering configurations is sealed against the thermostating fluid by a curved half-tube of aluminum visible in Fig. 3(a), which is glued to the inner surface of the stator. This is simpler and more efficient than the alternative method of passing the thermostating fluid through a fitted jacket within the stator, in which performance suffers from the thermal conduction barrier due to the unavoidable gap between the outer surface of the jacket and the inner surface of the quartz. In order to accomplish precise temperature control, a RTD temperature probe (3 mm diam) is introduced into the stator along the rotation axis through a slip fit O-ring seal and samples the thermostating fluid temperature just above the beam height. Using this probe as a control sensor our circulating temperature bath can maintain the temperature of the cell for our low viscosity aqueous surfactant samples within its own stability of $\pm$0.1 K for the data presented in this article.[30]

The mechanical performance specifications of our cell are shown in Table I. The cell rotor is driven by computer-controlled dc servo motors. At this stage, three motor/reducer

TABLE I. ORNL SANS Couette cell parameters.

Space requirements	25 cm wide×45 cm depth×70 cm height			
Motor	dc servo			
Stable rotational speed	~100–5000 rpm (direct drive) (available gear reductions 1:10, 1:100, 1:4096)			
Mean sample radius R	24.5 mm			24.75
Sample gap g	1.00 mm			0.50 mm
Conversion $\dot{\gamma}/f \cong 2\pi R/g$	2.6 s^{-1}/rpm			5.2 s^{-1}/rpm
Sample volume	14 ml			7 ml
Shear rate range[a]	without vap. bar. 0.01–12 500 s^{-1}	with vap. bar. 0.01–7500 s^{-1}	without vap. bar. 0.02–25 000 s^{-1}	with vap. bar. 0.02–15 000 s^{-1}

Note: The precision given for the rpm to average shear rate conversion factor reflects the change in shear rate across the gap discussed in Sec. II. For a Newtonian fluid the fractional change is about $2g/R$, or 4% and 8% for the 0.50 and 1.00 mm gaps, respectively.

[a]Maximum mechanical shear rates are shown. Assumes $\mathrm{Re} \equiv \rho \dot{\gamma}_{\max} g^2/\eta < \mathrm{Re}_{CR} \sim 1500$.

configurations are necessary to cover the entire shear range possible for a given gap. Each allows the shear rate to be varied by a factor of 50 for motor speeds in the range 100–5000 rpm. Thus the lowest reliable mechanical shear rate for our cell ~0.01 s^{-1} is reached with a gear reduction of 1:4096 at 100 rpm for the 1.00 mm gap (at a rotor frequency of 0.025 rpm). This system has the advantages of being relatively cheap and allowing smooth rotation over a very large dynamic range. It should be noted that digital drive options, stepper motors, or encoder controlled dc servos, can introduce significant jitter into the drive system at low shear rates to which some systems may be sensitive. Nevertheless, we plan in future to install such a system to reduce the inconvenience and, more importantly, the experimental delays and limitations imposed by the several drive changes necessary to cover the full shear rate range.

A direct mounted motor allows us to apply a maximum mechanical shear rate of 25 000 s^{-1} for the 0.50 mm gap at 5000 rpm, but our measurements are meaningful only if the sample is not affected by evaporation. With the active vapor barrier we found that the integrity of the evaporation-sensitive sponge samples[31] could be maintained for useful data acquisition times of several hours at a maximum shear rate of about 15 000 s^{-1} (3000 rpm for the 0.50 mm gap). This is over an order of magnitude better than was achieved with our original vertical vane design, which for the sponge measurements was limited to shear rates below about 1000 s^{-1}. In the old design, barrier failure occurred due to simple centrifugal expulsion of the well fluid. The well cap and angled vane of the new barrier allow us to operate up to a higher limit determined by turbulence in the vapor barrier fluid, which eventually causes rapid failure of the evaporation seal. Since the vapor barrier dimensions are slightly greater than the Couette gap and its geometry more complicated we can expect that critical Reynolds numbers for turbulent flow in the well will tend to be reached at lower rotation speeds than for the cell itself.[32] While a smaller vapor barrier will raise this limit it would also increase shear rates and viscous heating problems in a smaller volume of barrier fluid. The current design is certainly more accessible and convenient than a smaller barrier and is quite well matched to the capabilities of the Couette cell. It is also important to note that the operation of the vapor barrier will in general be extremely sample dependent. The sponge phases, which necessitated these design modifications (see Sec. IV), are critically sensitive to evaporation. They, therefore, present a fairly extreme test of the vapor barrier's performance. We note that in samples that are less sensitive to evaporation matching the vapor pressures of barrier and sample fluids will be less important, and the turbulence limit on performance may be increased by lowering the Reynolds number in the well at a given rotation speed by using barrier fluids of lower density or higher viscosity.

In addition to the problem of evaporation being particularly addressed in this work it is in general necessary to consider a number of sample dependent limits to the shear rate range for which reliable Couette SANS measurements are possible. Unlike mechanical limitations such as minimum or maximum motor control speeds or limitations on motor torque these can easily be mistaken for shear-induced structural responses. As noted above shear heating is a known problem, particularly for samples with higher viscosities (e.g., polymeric solutions) or lower thermal conductivities (e.g., organic solvents). As the shear rate is increased the viscous heating of the sample can outstrip the cooling power[30] of the cell and the corresponding increase in temperature may cause structural changes in the sample. In measurements at temperatures close to a sample phase boundary this effect might even drive a phase transition in the sample volume.[33] Such effects may be offset if the cooling power of the temperature control circuit is increased by operating the temperature bath fluid at a temperature somewhat below the target temperature of the sample. However, in such cases, a temperature reading from within the sample is necessary for reliable sample temperature monitoring and control. In our current design, it would be difficult to introduce a probe directly into the sample volume at the beam height without compromising the flow characteristics of the cell. In a future stator design we do intend to introduce a small temperature probe (such as a thermistor ~1 mm diam) at the point of the stator cone. While not ideal this will improve sample temperature control for such samples by allowing direct temperature monitoring of the sample volume.

Similarly, although the choice of outer cylinder rotation

for a Couette cell eliminates the possibility of classic Taylor secondary flow, for fluids with significant storage moduli (e.g., viscoelastic polymer and surfactant solutions) elastic instabilities which cause fine, time periodic cellular flows are still possible. As for turbulence this departure from laminar flow would lead to disorder in a scattering pattern that might be misinterpreted as microscopic structural response to the supposedly still laminar shearing flow. The onset of these instabilities depends on a critical value of the Deborah number, where $\mathrm{De} \equiv \tau\dot{\gamma}$ is defined as the product of a sample's characteristic relaxation time and the shear rate. Larson and co-workers[34] have investigated these instabilities in viscoelastic fluids under Taylor–Couette flow. For the gap ratios in our cells (g/R of 0.02 and 0.04) their work indicates that the critical Deborah number for our Couette cell is about 40.

In all cases it is necessary to evaluate Couette SANS scattering results critically on a sample by sample basis to ascertain whether they truly reflect shear-induced changes or may be more simply explained by uncontrolled secondary effects.

III. NEUTRON SCATTERING: REDUCTION TO ABSOLUTE SCALE

The SANS measurements presented here were performed on the NG-3 SANS spectrometer at the NIST Center for Neutron Research in Gaithersburg, Maryland. The incident neutron wavelength used was 0.6 nm with $\Delta\lambda/\lambda$ of 15%. A prealigned aperture package allows the Couette sheared sample to be measured in three standard scattering configurations [Fig. 3(b)]. As noted above, in the usual radial scattering configuration, the neutron beam passes through the sample along the velocity gradient direction, while in the tangential configuration, the beam passes along the flow direction through the side of the cell. A third standard option allows the beam to pass through the sample at 45° to the flow and gradient directions. The apertures defining the three incident beam positions (radial, 45°, and tangential) are machined into a single 1-mm-thick cadmium sheet. In the radial configuration the beam is defined by a 10-mm-diam circular aperture. In the tangential, the rectangular apertures are 12 mm high and 0.66 mm and 0.25 mm wide for a 1 mm or 0.5 mm gap, respectively. A rectangular aperture 10 mm high and 4 mm wide is available in the 45° configuration for both gaps. To reduce background the cadmium sheet defines only the edges of the beam and is mounted behind guard apertures in a boron carbide doped epoxy resin to take advantage of the softer ^{10}B neutron absorption gamma ray. This aperture package is fixed to stages allowing vertical and horizontal translation for precise slit alignment and is mounted on the horizontal plate supporting the stator. The tangential configuration is the most sensitive to alignment and is used as the reference position of the cell. After the slit package has been aligned with the Couette cell and the spectrometer in this configuration, changing between configurations is a simple matter of moving the cell the known distances between the aperture centers. Measurement times will be generally dependent on the sample scattering volume, which is greatest for the radial configuration and least for the tangential. In the data presented below typical times are 5, 10, and 25 min for the radial, 45°, and tangential configurations, respectively.

As in conventional SANS data reduction[35] each of our raw data sets was corrected for detector background, sensitivity, and scattering from the empty cell. In the radial configuration, the transmission necessary for absolute normalization was determined from the ratio of the unscattered beam intensities through the sample loaded and empty Couette cell and the known sample thickness (twice the Couette gap). Placing off-radial data on an absolute scale, especially in tangential geometry where the sample thickness is extremely sensitive to alignment, is more problematic, and indeed is usually ignored. In the rare instances where it is attempted, it has been done by initially determining a scale factor between absolutely scaled radial scattering data from *isotropic* scattering from the sample and a corresponding tangential measurement. This scaling factor is then applied uniformly to all subsequent tangential scattering measurements.[36] We present here an alternative approach, which may be used even if no reliable isotropic scattering data is available; as, for instance, in the case of some liquid crystals for which even loading the cell will introduce some unavoidable shear alignment.

Our method for placing tangential and other off-radial data on an absolute scale relies on the determination of the effective sample thickness in these configurations. With this and a direct beam measurement made in the same geometry, one can reduce the data in the normal fashion. Experimentally, one can use the radial transmission to determine the absorption coefficient μ of the solution from $T_{\mathrm{rad}} = \exp[-\mu t]$, where the known sample thickness $t = 2g$ is twice the Couette gap, so $\mu = -\ln[T_{\mathrm{rad}}]/2g$. The experimentally determined tangential transmission can then be used to determine the effective thickness of the sample in this configuration:

$$t_{\mathrm{eff}} = -\ln[T_{Tgt}]/\mu = 2g\,\ln[T_{Tgt}]/\ln[T_{\mathrm{rad}}].$$

The same method can also be applied to any arbitrary off-radial configuration. Figure 4 shows macroscopic differential cross sections $d\Sigma/d\Omega$ (in cm^{-1}) determined for 3% and 7% sponge phases. Shown are conventionally reduced static (Hellma) cell SANS data and Couette radial geometry scattering measurements, as well as tangential and 45° configuration scattering data reduced using the procedure described above. The good quantitative agreement between two methods shows the effective thickness determination works well in converting scattered intensities into absolute cross sections for these off-radial geometries.

By translating the slit across the tangential position with the cell empty an accurate alignment may be achieved by noting the sharp transmission rise when the beam initially intercepts the gap at the rotor cylinder's inner radius and the sharp decrease when it reaches the quartz again at the outer radius of the stator (Fig. 5). In this figure, we show the measured transmitted intensity of the beam defined by the 0.66-mm-width sample aperture through the cell sample with the 1.00 mm gap compared to a theoretical calculation. The path length for rays of the direct beam through a quartz path passing at a distance r from the cell's axis of rotation $t_Q[r]$ was

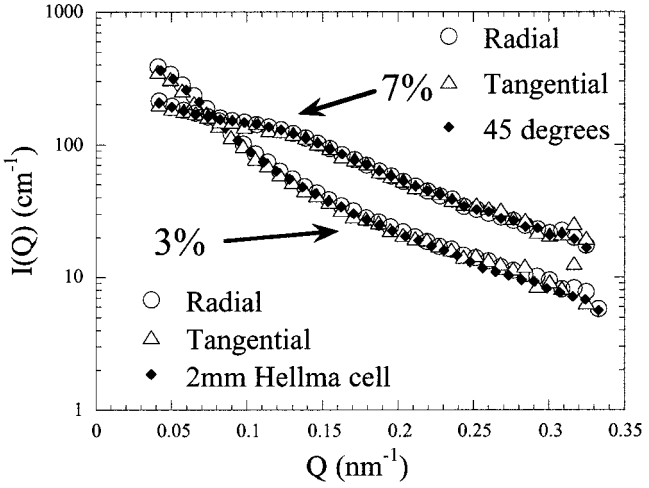

FIG. 4. Scattered intensity $d\Sigma/d\Omega$ (in cm^{-1}) for a 3% and 7% sweetened sponge phase determined for different configurations at zero shear. For 3%: Couette cell measurements in (○) radial configuration and (△) tangential configuration compared to conventional (◆) 2 mm Hellma cell SANS measurement. For 7%: Couette cell measurements in (○) radial, (△) tangential, and (◆) 45° configurations. The non-radial Couette configurations were absolutely normalized of by the effective thickness method described in the text.

calculated from simple geometrical considerations and the transmission for each ray transmission according to $T_Q = \exp[-\mu_Q t_Q(r)]$, where μ_Q is the absorption coefficient of the quartz ($\mu_Q = 0.23$ cm^{-1} for the 6 Å neutrons used in this measurement).[37] The solid line curve is a plot of $\langle T_Q \rangle$, a numerical average of the transmission across the slit width.

For this precise cell alignment we were able to check the effective sample thickness determined from the transmission when the cell was loaded. It agreed to ~5% with a calculation of a simple average of the path lengths through the sample annulus. A comparable variation of about 3% was observed in effective thicknesses determined from samples of differing transmissions loaded using the same tangential alignment of the cell. As noted above this technique can be applied somewhat more generally than the uniform scaling method described above since SANS transmission measurements are insensitive to alignment of anisotropic scattering centers in the sample.

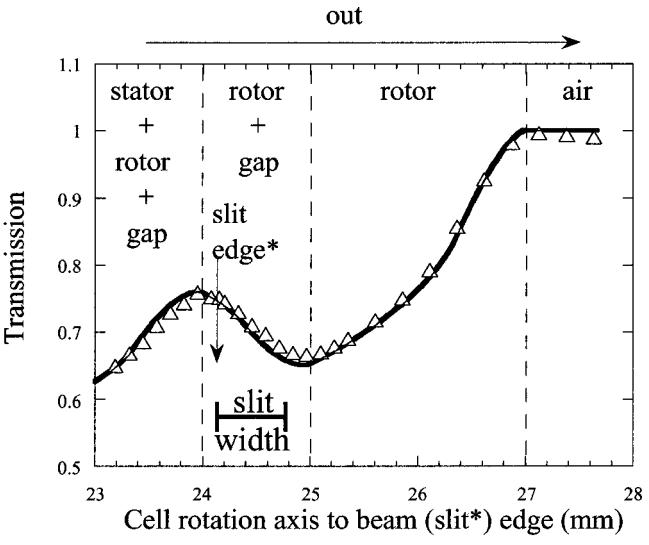

FIG. 5. Transmission variation as the beam defining slit is translated across the tangential position with the cell empty for the 1.00 mm gap. The sharp changes in the curve correspond to interception of material boundaries by the neutron beam. The continuous line represents average transmission across the beam calculated as described in the text. The final slit edge position used for the Couette cell SANS measurements in this case is indicated by the arrow.

IV. EXPERIMENTAL RESULTS

The performance of our Couette cell design may be illustrated by a brief discussion of recent experimental results on a sponge phase under shear. A full description of this work is published elsewhere.[38]

In a recent publication, Mahjoub and co-workers[23] reported x-ray measurements which they interpreted as indicating that a relatively concentrated sponge phase (10% to 15% Cetylpyridinium chloride/hexanol membrane in brine) was totally transformed into a lamellar phase by applied shear rates of ~20 s^{-1} in a Couette cell. The observed transition was first order with the lamellar phase initially nucleating into the sponge phase in the *a* orientation (lamellae perpendicular to the cell rotation axis, i.e., the shear vorticity direction), as the shear was increased they reported a reorientation to the *c* orientation (lamellae perpendicular to the shear gradient direction) above a certain shear rate. Moreover, the induced lamellar phase was reported to be stabilized at high shear with no evidence of relaxation to its supposed thermodynamic equilibrium state: the original sponge phase.

Theoretical treatments[39] indicate that sponge to lamellar transitions should occur for a critical shear rate $\dot{\gamma}_c \approx k_B T/\xi^3 \eta$, where ξ is the characteristic dimension of the sponge (inversely proportional to the membrane volume fraction ϕ), k_B is Boltzmann's constant, T is the temperature, and η the solvent viscosity. The first order nature of the transition reported by Mahjoub *et al.*[23] and the initial *a* orientation of the lamellae are consistent with the theory. However, for a 10% membrane volume fraction sponge phase their values of $\xi \approx 33$ nm and $\eta_s \cong 1$ cP give an expected value for $\dot{\gamma}_c$ of order 100 000 s^{-1}. This is about four orders of magnitude higher than their observation.

Initially we attempted to replicate these results using the NIST Couette shear cell.[14] This shear cell is equipped with a simple vertical vane vapor barrier. While initially no structural effects of shear were seen, we soon observed scattering changes indicating an apparent shear-induced sponge to lamellar phase transitions at low shear rates. Also, we did not find these transitions to depend reproducibly on shear rates. However, we did find them to be strongly dependent on the shearing history of the sample and rather simply on its time within the cell. Further, in each case where a transition was observed, samples recovered from the cell were found to be in a macroscopic biphasic state L_α/L_3. If we simply ignored this biphasic nature of the final state we were able to duplicate most of the results of Majhoub *et al.*,[23] including an apparent shear-induced sponge to lamellar transition with a long relaxation time and a flip reorientation of the lamellar phase from perpendicular to parallel alignment. However, by instituting a protocol whereby we began at low shear rates

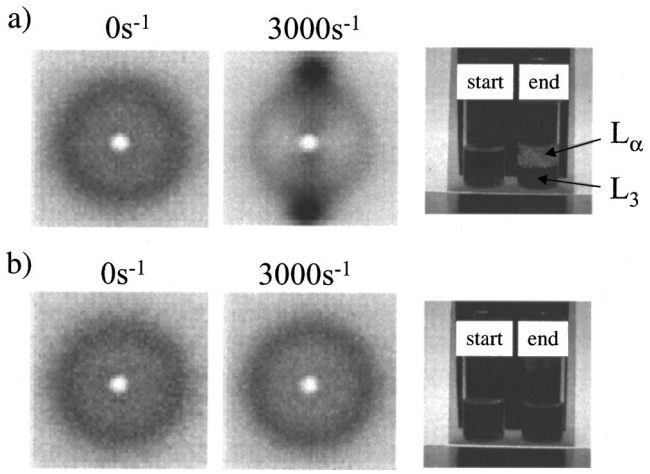

FIG. 6. Neutron scattering pattern for a 15% CPCl/hexanol volume fraction in brine (0.2 M NaCl) at rest and under 3000 s^{-1} performed with (a) the previous and (b) the updated vapor barrier. The photographs are recovered samples compared with fresh samples from the batch solution in crossed polarizer views. For the sample recovered from the old vapor barrier cell a significant lamellar phase (L_α) component is seen floating above the sponge phase (L_3).

and progressively increased the shear rate until a transition was observed, then stopped and replaced the sample with a fresh sample and continued on from the previously attained shear, we were able to traverse the entire shear range (0 to 6000 s^{-1}) without observing any transition at all. Each sample that displayed a transition was clearly biphasic when removed and remained so upon shaking, but could be returned to the sponge phase by adding a very small drop of hexanol.

Careful inspection of the phase diagram for this system[19–22,40] shows that the sponge phase is extremely sensitive to hexanol concentration while being almost completely insensitive to water evaporation. It became clear to us that our results and those reported by Mahjoub *et al.*[23] were much more simply explained by concentration driven first order transitions due to the evaporation of hexanol, rather than true shear-induced transitions.[24] To fully test this hypothesis we needed a more effective Couette vapor barrier which would operate the several hours at high shear rates necessary for a complete shear experiment. This lead us to the improvements of the ORNL Couette cell design presented above. Figure 6 compares radial scattering patterns of the 15% sponge phase at rest and under a shear rate of 3000 s^{-1} obtained with its old vertical vane and angled vane vapor barrier. Using the old design, Bragg peaks along the vorticity axis indicate lamellar phase alignment in the horizontal *a* orientation within the cell. When removed, the sample was clearly biphasic. When observed between crossed polarizer, the birefringent L_α phase was seen floating over the isotropic L_3. For the new design we observed no distortion of the isotropic correlation ring, suggesting that shearing at this rate does not affect the geometry of this phase, just as one would expect from theory. The recovered sample was not in this case birefringent. When observed between crossed polarizers it was indistinguishable from another sample taken from the original batch. With the vapor barrier of the new cell eliminating spurious evaporation effects we observed no change in the scattering from this sample to shear rates as high as 10 000 s^{-1}.

These results are consistent with the theoretical prediction of critical shear rates for this system $\sim$100 000 s^{-1}, which is well beyond the operational limits of our cell. The scaling of the theory[39] suggests that experimentally achievable transition shear rates require either increasing the correlation length of the sponge phase or increasing its solvent viscosity. Diluting the sponge will increase the correlation length. However, the decreasing width of sponge phase stability domain with dilution, a loss of signal strength in the sponge scattering ring, and its movement to lower scattering vector, as well as greatly increased sensitivity to cosurfactant evaporation make the dilution option impractical. We have, therefore, adopted the alternative strategy of increasing the solvent viscosity. We take our lead from work indicating that in microemulsion systems adding sugar can achieve this result without altering the form of the phase diagram.[41] We have found that the viscosity of the sponge phase in the system CPCl/hexanol/brine can be increased by an order of magnitude by simply dissolving sugar in the brine.[42]

Figure 7 shows radial and tangential scattering patterns for a 10% sponge phase sweetened with 40 vol % of dextrose in the brine solvent. The addition of this sugar raises the solvent viscosity by over an order of magnitude (1 to 13 cP). At zero or low shear rates an isotropic ring is observed for both configurations. The ring peaks at a scattering vector $Q_\xi \approx 0.018\,\text{Å}^{-1}$ characteristic of the correlation length size of passages $\xi = 2\pi/Q_\xi \approx 350\,\text{Å}$ in the convoluted sponge membrane morphology. As the shear rate increases, the scattering profile becomes increasingly anisotropic and the correlation ring in the radial scattering data decreases in intensity. This decrease is more rapid in the scattering along the vorticity axis (*Z*). (This is consistent with previous radial scattering measurements made by Diat and Roux[43] and Safinya and co-workers.[13]) In the tangential geometry the scattering signal increases along the flow velocity gradient direction (∇V) and shifts toward higher wave vector. At 3400 s^{-1}, fully formed Bragg peaks at $\sim$0.021 $Å^{-1}$ indicate the formation of a shear-induced lamellar phase with a smectic periodicity of $\sim$300 Å with membranes aligned parallel to the Couette cell walls (i.e., layer normals point along ∇V).

Whether or not sugar is added, the phase behavior of this system is extremely sensitive to hexanol evaporation and use of the vapor barrier was essential to obtaining reliable repeatable results for this system. When the barrier was used, the anisotropic shear-induced scattering pattern immediately returned to the previously observed isotropic pattern upon cessation of shear. This spontaneous relaxation of the sheared sample to the sponge phase is contrary to the observations of Mahjoub *et al.*[23] on the sugar-free system. As the vapor barrier prevents evaporation in our case, the sample was found to still be wholly in the sponge phase when recovered from the cell. With careful operation of the vapor barrier, no history dependent effects were observed for these systems. Shearing a presheared sponge phase repeatably yields the same response. More details about the mechanisms involved in the observed transitions will be presented elsewhere.[38]

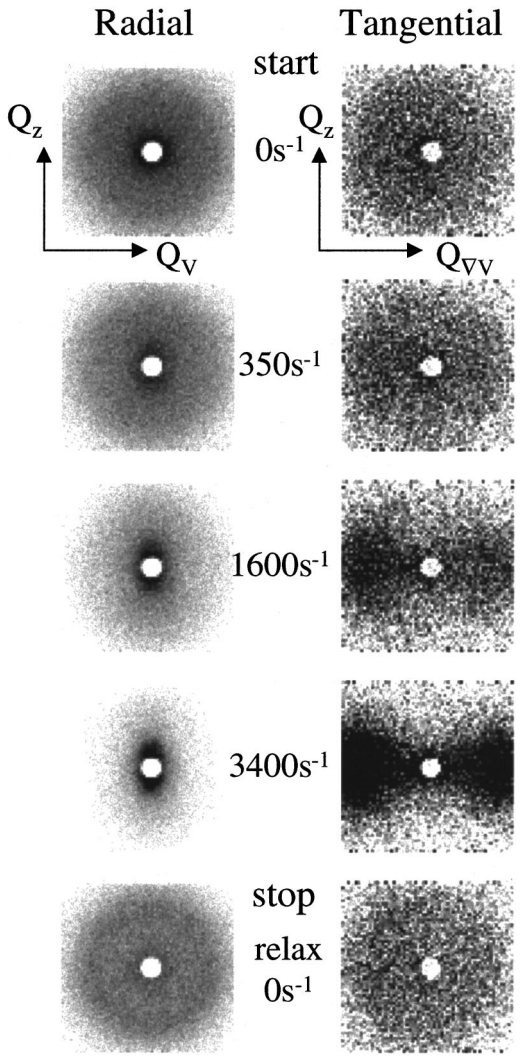

FIG. 7. Neutron scattering pattern for a 10% sweetened sponge phase (40% sugar volume fraction in brine) in radial and tangential configurations at a range of shear rates. After cessation of shear the induced lamellar phase relaxes instantly to the sponge structure. The slight asymmetry visible in the tangential configuration scattering patterns occurs because neutrons scattered toward the cell axis will traverse a longer path through the sample fluid than those scattered away.

ACKNOWLEDGMENTS

Our thanks to D. Glandon, B. Taylor of ORNL, and G. Porte of the University of Montpellier, France. Oak Ridge National Laboratory is managed for the U.S. Department of Energy by UT-Batelle LLC under Contract No. DE-AC05-00OR22725. The NG3 SANS instrument at the National Institute of Standards and Technology Center for Neutron Research is supported by the U.S. National Science Foundation under agreement DMR-9423101. Identification of equipment or materials does not imply recommendation by NIST. G.G.W. acknowledges support from the Australian Nuclear Science and Technology Organization and the Australian Research Council.

[1] B. J. Ackerson and N. A. Clark, Phys. Rev. A **30**, 906 (1984).
[2] P. D. Butler, Curr. Opin. Colloid Interface Sci. **4**, 214 (1999), and references therein.
[3] E. Cappelaere, J. F. Berret, J. P. Decruppe, R. Cressely, and P. Lindner, Phys. Rev. E **56**, 1869 (1997).
[4] P. D. Butler, L. J. Magid, W. A. Hamilton, J. B. Hayter, B. Hammouda, and P. J. Kreke, J. Phys. Chem. **100**, 443 (1996).
[5] O. Diat, D. Roux, and F. Nallet, J. Phys. II **3**, 1427 (1993).
[6] J. Zipfel, J. Berghausen, P. Lindner, and P. Richtering, J. Phys. Chem. B **103**, 2841 (1999).
[7] O. Diat and D. Roux, J. Phys. II **3**, 9 (1993).
[8] P. Panizza, A. Colin, C. Coulon, and D. Roux, Eur. Phys. J. B **4**, 1496 (1998).
[9] P. Sierro and D. Roux, Phys. Rev. Lett. **78**, 1496 (1997).
[10] P. Linder and R. C. Oberthur, Rev. Phys. Appl. **19**, 759 (1984).
[11] J. A. Pople, I. W. Hamley, and G. P. Diakun, Rev. Sci. Instrum. **69**, 3015 (1998).
[12] Ch. Munch and J. Kalus, Rev. Sci. Instrum. **70**, 187 (1999).
[13] R. J. Plano, C. R. Safinya, E. B. Sirota, and L. J. Wenzel, Rev. Sci. Instrum. **64**, 1309 (1993).
[14] G. C. Straty, H. J. M. Hanley, and C. J. Glinka, J. Stat. Phys. **62**, 1015 (1991). Later modified by NIST to include a vertical vane vapor barrier and conical bottom.
[15] G. C. Straty, C. D. Muzny, B. D. Butler, M. Y. Lin, T. M. Slawecki, C. J. Glinka, and H. J. M. Hanley, Nucl. Instrum. Methods Phys. Res. A **408**, 511 (1998).
[16] S. M. Baker, G. Smith, R. Pynn, P. Butler, J. Hayter, W. Hamilton, and L. Magid, Rev. Sci. Instrum. **65**, 412 (1994).
[17] R. K. Prudhomme and G. G. Warr, Langmuir **10**, 3419 (1994).
[18] M. Kisilak, H. Anderson, N. S. Babcock, M. R. Stetzer, S. H. J. Idziak, and E. B. Sirota, Rev. Sci. Instrum. **72**, 4305 (2001).
[19] R. Gomati, J. Appell, P. Bassereau, J. Marignan, and G. Porte, J. Phys. Chem. **91**, 6203 (1987).
[20] G. Porte, J. Marignan, P. Bassereau, and R. May, J. Phys. (Paris) **49**, 511 (1988).
[21] G. Porte, J. Appell, P. Bassereau, and J. Marignan, J. Phys. (France) **50**, 1335 (1989).
[22] Y. Nastishin, E. Lambert, and P. Boltenhagen, C. R. Acad. Sci. Paris **321**, 205 (1995).
[23] H. F. Majhoub, C. Bourgaux, P. Sergot, and M. Kleman, Phys. Rev. Lett. **81**, 2076 (1998).
[24] P. D. Butler, L. Porcar, W. A. Hamilton, and G. G. Warr, Phys. Rev. Lett. **88**, 059601 (2002).
[25] Widmad Glass, 1002 Harding Highway P.O. Box 688, Buena, NJ 08310.
[26] Creavey Seal Company, Olyphant, PA.
[27] See, for instance, C. W. Macosko, *Rheology: Principles, Measurements, and Applications* (Wiley-VCH, Weinheim, 1994), Chap. 5, Sec. 3.
[28] G. I. Taylor, Proc. R. Soc. London, Ser. A **157**, 546 (1936); L. D. Landau and E. M. Lifshitz, *Fluid Mechanics*, 2nd ed. (Pergamon, London, 1987), Sec. 27.1, p. 99.
[29] P. G. De Gennes, J. Chem. Phys. **60**, 5030 (1974).
[30] Following Lindner and Oberthur (Ref. 10), we assume that for our cell the total heat created may be removed through the stator as the circulating bath fluid and the sample are both in direct contact with the inner quartz cylinder over a common area of about 60 cm^2. The shear heating power to the sample $P \approx V\eta\dot{\gamma}^2$, where V is the sample volume, must be removed by the cooling circuit so $P \approx \dot{l} C_p \Delta T$, where $\dot{l}$ and C_p are the flow rate and the heat capacity of the circulating bath fluid and ΔT is the temperature difference, which can therefore be maintained below a critical viscosity: $\eta_{\text{crit}} \sim \dot{l} C_p \Delta T / V\dot{\gamma}^2$. For our bath the circulation rate of water ($C_p = 4.2\ \text{K}^{-1}\ \text{g}^{-1}$) through our cell stator is about 50 gs^{-1} (31/min), so $\Delta T \approx 0.1$ K can be maintained for a cell volume $V \sim 10\ \text{cm}^{-3}$ at $\dot{\gamma} = 3400\ \text{s}^{-1}$ up to a viscosity of about 200 cP. This is an order of magnitude higher than the viscosity of the 10% membrane volume fraction sweetened sponge phase at this shear rate for which SANS data is presented in Fig. 7 of Sec. IV, which has the highest viscosity of the samples presented in this article.
[31] These limit shear rate tests were performed on unsweetened sponge phase samples, which have viscosities of a few cP [P. Snabre and G. Porte, Europhys. Lett. **13**, 641 (1990)], rather than the higher viscosity sweetened sponges discussed in the previous note (Ref. 30) for which viscous heating would become a significant problem at these high shear rates.
[32] Taylor vortex flow will obviously occur at much lower shear rates for the fluid between the inner wall of the well and the stationary vane. While the circulation of this regular flow pattern probably degrades the long-term performance of the barrier, it does not cause a catastrophic failure. From our observations, it also seems that the barrier continues to seal (in that the integrity of evaporatively sensitive sponge phases in the sample cell con-

tinues to be maintained) even with some degree of turbulence being evident in the barrier well.
[33] It should be noted that for Couette SANS studies one of the advantages of the CPCl/hexanol/brine sponge phases for which we present data in Sec. IV is their thermal stability, which makes them insensitive to viscous heating effects. See, for instance, C. Quilliet, M. Kleman, M. Benillouche, and F. Kalb, C. R. Acad. Sci. Paris **319**, 1469 (1994).
[34] R. G. Larson, E. S. G. Shaqfeh, and S. J. Muller, J. Fluid Mech. **218**, 573 (1990).
[35] G. D. Wignall and F. S. Bates, J. Appl. Crystallogr. **20**, 28 (1986).
[36] J. Penfold, E. Staples, A. Khan Lodhi, I. Tucker, and G. J. T. Tiddy, J. Phys. Chem. B **101**, 66 (1997).
[37] The absorption coefficient of the quartz was determined from a transmission measurement for 6 Å neutrons through the empty cell in the radial geometry for which the path length through the quartz is essentially constant at 8.00 mm (4×2.00 mm) across the width of the beam.
[38] L. Porcar, W. A. Hamilton, P. D. Butler, and G. G. Warr (in preparation).
[39] M. Cates and S. T. Milner, Phys. Rev. Lett. **62**, 16 (1989).
[40] H. F. Majhoub, K. M. McGrath, and M. Kleman, Langmuir **12**, 3131 (1996).
[41] V. Chen, Ph.D. thesis, University of Minnesota 1988.
[42] L. Porcar, W. A. Hamilton, P. D. Butler, and G. G. Warr (in preparation).
[43] O. Diat and D. Roux, Langmuir **11**, 1392 (1995).